General Proposal

T-REX: Time-Resolving Explorer Satellite

Time-Resolving Supermassive Black Holes from Low-Earth Orbit

Ref Bari[a] **Amelia Frickey**[a] **Graham Neely**[a] **Kaylee DeGennaro**[a] **Sharanya Palit**[a] **Sebastian Abreu**[b] **Noah Barton**[a] **Lucas Anderson**[c] **Jeremy Goodman**[d]

[a] *Brown University*
[b] *Columbia University*
[c] *Utah State University*
[d] *Princeton University*

E-mail: refath_bari@brown.edu

Abstract: We present T-REX: The Time-Resolving Experiment, a proposed SmallSat which seeks to capture the first time-resolved movie of Sgr A^* at 86 GHz. T-REX will achieve a 22-min temporal resolution by leveraging a Low-Earth Orbit Very-Long-Baseline-Interferometry (VLBI) SmallSat platform. T-REX will constrain Sgr A^*'s spin to $\leq 10\%$ ground truth by capturing time-resolved videos of Sgr A^*. T-REX will operate at $\lambda \sim 3.5mm$ with a $d \sim 2.5$m antenna operating at a primary receiver temperature of ~ 20K, with a frequency bandwidth $\Delta f_{BW} = 32$ GHz. By virtue of its sub-ISCO temporal resolution, T-REX will also enable parameter estimation on transient astrophysical phenomena by capturing time-resolved videos of black hole accretion disks, quasi-periodic outbursts, relativistic jets from AGN, and tidal-disruption events. T-REX will achieve a maximum angular resolution $35\mu as$ in addition to its 22-minute temporal resolution. T-REX would be enabled by state-of-the-art laser downlink communications systems and ultra-stable oscillators which enable a LEO VLBI SmallSat platform. By leveraging extensive ground and space supporting infrastructure, T-REX will capture the first time-resolved movie of Sgr A^*. This proposal presents the primary science objectives, engineering constraints (SWaPC requirements), mission parameters, concept of operations (ConOps), and instrumentation breakdown for T-REX.

ArXiv ePrint: 1234.56789

Contents

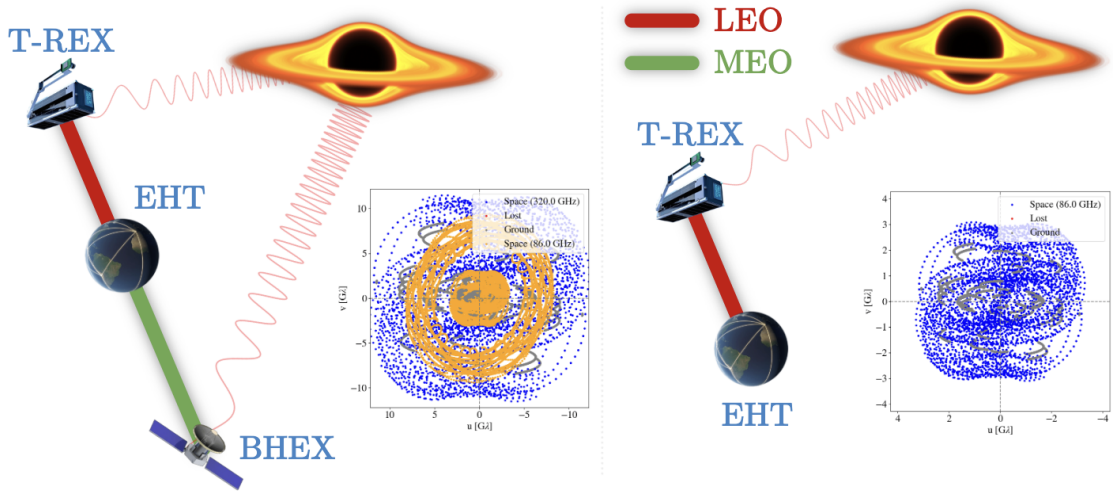

Figure 1: T-REX will capture time-resolved videos of black hole targets from LEO

1 Primary Science Objectives

In 2019, the Event Horizon Telescope (EHT) directly imaged the black hole M87* with an angular resolution of $\sim 23\mu as$ at 230 GHz [1]. The T-REX (Time-Resolving Experiment) mission seeks to take the next leap: Capturing the first video of a black hole. T-REX will be an 87 kg, $25 million radio VLBI satellite in low-earth orbit operating at 86 GHz, supporting NASA & NSF's "highest-priority sustaining activity [which] is a space-based time-domain and multi-messenger program of small and medium scale missions." [2] The Primary Science Objectives of the T-REX mission are as follows.

- **Capture Time-Resolved Videos of Sgr A* & M87**
  - *Goal:* Constrain Mass and Spin of Sgr A* and M87 to $< 10\%$ of ground truth
  - *Observations:* Our time-resolved video and polarimetry will jointly constrain the mass and spin of the black hole via periodic brightness modulations in the movie [3–5]. Matching a measured variability period $t_{\rm var}$ to the orbital period T_{orb} gives

$$M = \frac{c^2 D}{G}\frac{\theta_{sh}}{\mathcal{F}(a,i)}, T_{\rm orb}(r,a) = \frac{2\pi GM}{c^3}\left(r^{3/2} \pm a\right) \tag{1.1}$$

    T_{orb} yields the spin $\chi = a/M$ once M is fixed from the shadow θ_{sh} [6, 7].

- **Characterize dynamics of transient astrophysical events on ≤ 12 hr timescales.**
  - *Goal:* Monitor tidal disruption events, quasi-periodic outbursts, and nHz-frequency binary black hole systems with sub-ISCO[1] temporal resolution. Of particular interest is OJ 287 [8], a binary system which can be simultaneously co-observed by a radio telescope (T-REX) and a gravitational wave observatory (PTA) [9, 10].
  - *Observations:* Monitor flares, outbursts, and variability in radio targets to characterize the orbital dynamics of black holes in these systems [11].

- **Survey of Bright AGN at 86 GHz**
  - *Goal:* Conduct a population study of radio-loud AGN targets at 86 GHz to characterize their emission profiles, variability, and luminosity.
  - *Observations:* T-REX's 86 GHz movies of AGN targets will enable qualitative characterization of accretion flow and constraints on the magnetic field strength and jet power of AGN targets. The Blandford-Znajek mechanism predicts that the power released by relativistic jets $P_{BZ} \propto \chi^2$ [12]. The synchrotron self-absorption turnover gives the transverse field via $B_\perp\,[\mathrm{G}] \approx 10^{-5}\, b(\alpha)\, \frac{\theta_{\rm mas}^4\, \nu_{\rm GHz}^5}{S_{\rm Jy}^2}$ [13]. Combining with B_z yields the toroidal component B_ϕ. The polarization-fraction spectrum and SED fixes the electron–ion temperature ratio T_e/T_i (guided by GRMHD/PIC) [14]. Finally, time-domain morphology (pattern speeds $\Omega_p = d\phi/dt$ of bright features at 22-minute cadence) distinguishes winding material spirals (tracking local Ω_K) from quasi-stationary density waves [15].

[1] We refer to sub-Sgr A^* ISCO here as timescales on the order of ≤ 30 min.

2 Engineering Constraints

	Antenna	Receiver	Cryocooler	Solar Panels	USO	Backend	Terminal	**T-REX**
								
Size	$\sim 2.5m$	$\sim 0.02m^3$	$754mm \times 146mm \times 300mm$	$1U(100mm \times 100mm \times 100mm)$	$60mm \times 60mm \times 32mm$	$12mm \times 12mm$	$3U(300mm \times 300mm \times 300mm)$	N/A
Weight	$\sim 25-50kg$	$5-7kg$	$22kg$	$1.2kg$	$\sim 1kg$	$\sim 1kg^*$	$3kg$	$\sim 85.3kg$
Power	$10-20W$ (deployment)	$\sim 10W$	$300W$ $400mW@15°K$	$100W$ generated	$\sim 3W$	$\sim 4W$	$100W$	$\sim 437W$
Cost	\$2 – 5Mln \$4 – 11Mln	$\sim$ \$1mln	\$10mln	$\sim$ \$100k	$\sim$ \$1mln*	$\sim$ \$1mln*	$\sim$ \$1mln*	$\sim$ \$25mln

Figure 2: Preliminary T-REX Size, Weight, Power, and Cost Requirements

The development of T-REX requires several technical constraints:

- **Antenna Accuracy & Pointing**
  - *Requirements:* T-REX's $2.5m$ diameter antenna must have a pointing accuracy $< 30as$, surface accuracy $< 40\mu m$, and aperture efficiency $\eta_A \sim 85\%$ to achieve $SNR > 5$. If operating in the single-dish mode, T-REX has a nominal angular resolution $\theta \sim 4.8$ arcminutes, clearly necessitating VLBI for sub-arcminute θ_{FOV} for black hole targets [16].
  - *Challenges:* By virtue of being in LEO, the antenna must rapidly slew to remain line-of-sight on the same target. Furthermore, infrared emissions are more significant at LEO, requiring exquisite thermal control onboard the satellite [17].
- **Data Downlink from LEO**
  - *Requirements:* The famous ground coverage problem for LEO satellites is exacerbated by the remarkable amount of data generated by VLBI. Assuming a $f_{duty} = 0.5$ duty cycle for a 5400 s (90-minute) orbit in LEO, T-REX would generate $\sim 10,800$GB of data over a single orbital period.
  - *Challenges:* A MEO orbit has sufficient ground coverage with just 4 ground stations [18]. However, a LEO orbit spends only $t \sim 5$ minutes within the observing cone of any given station, necessitating a three-tiered solution: Secure more ground stations[2], downlink at $> 100Gb/s$[3], and record data onto physical SSD storage onboard the satellite between downlink passes.

[2]We are currently collaborating with the University of Western Ontario on the CSA FAST grant on upgrading their ground radio terminal to an optical terminal for T-REX.

[3]We are corresponding with MIT Lincoln Laboratory regarding potentially developing a derivative of their TBIRD CubeSat, which achieved downlink rates of $200Gb/s$ from LEO in 2022.

3 Mission Parameters

T-REX will be situated on a circular low-earth orbit ($r \sim 400$km) with high orbital inclination $i > 80°$ to maximize ground coverage. The mission parameters are outlined below:

- **System Equivalent Flux Density (SEFD)**
  - *Requirements:* Using representative values for $A \sim 4.9m^2$ and a conservative system temperature $T^*_{sys} = [T_{rx} + \eta_{ff} T_{b,inc}](1 + r) \sim 100K$[4]

$$\text{SEFD}_{\text{T-REX}} = \frac{2kT^*_{sys}}{\eta_A A} \sim 66,000 \text{ Jy} \tag{3.1}$$

    In comparison, $\text{SEFD}_{\text{BHEX}} \sim 18,000$ Jy [19] and $\text{SEFD}_{\text{SMT}} \sim 10,500$ Jy [20].

- **Thermal Noise**
  - *Requirements:* T-REX will have two baselines[5]: A Space-Space baseline from T-REX to BHEX b_{ss} and a Space-Ground baseline from T-REX to EHT b_{sg}. The thermal noise on each baseline is

$$\sigma_{\text{T-REX - EHT}} = \frac{1}{\eta_Q} \sqrt{\frac{\text{SEFD}_{\text{T-REX}} \text{SEFD}_{\text{EHT}}}{2\Delta\nu\Delta t}} \tag{3.2}$$

    Using representative values for $\eta = 0.75, \Delta\nu = 32$ GHz, $\Delta t_{ss} = 100s$[6] gives

$$\sigma_{\text{T-REX - BHEX}} \sim 12.65 \text{ mJy}, \sigma_{\text{T-REX - EHT}} \sim 40 \text{ mJy} \tag{3.3}$$

- **Frequency Reference System**
  - *Requirements:* VLBI requires an exquisite means of tracking the exact time-of-arrival for radio signals hitting the antenna. A LEO VLBI platform requires coherence loss $L < 10\%$ and phase error $\Delta\phi < 1°$. We found that the phase error requirement was nominally met by the Ultra-stable Oscillator (USO) under development for the LISA mission, which has $\sigma_t = 8 \cdot 10^{-15}$ [21]. The coherence loss requirement is met by ESA's JUICE USO, which gives $L \sim 1\%$ [22].

- **Data Payload**
  - *Requirements:* The data generation rate is $\text{Rate(bps)} = N_{\text{bits}} \times \Delta\nu \times 2_{\text{pol}} \times 2_{\text{Nyquist}}$ [23], which (assuming a $T_{obs} = .5T_{orb}$ duty cycle), gives 43, 200GB data generated in an orbit. Assuming a 64 GB/s downlink rate with a cumulative ground contact window of $600s$ results in $\sim$ 1250GB left onboard the satellite. We compute the cumulative "lost" bits by integrating and removing $R_{\text{loss}} = 64 \times 10^9$ b/s across each contact window.

[4] $T_{rx} = 15K$ is T-REX's receiver temperature and $T_{b,inc} = \frac{F_{tot} A_{eff}}{2k}$ is the incident brightness temperature of the antenna due to observing a given target. BHEX has $T_{sys} = 50K$ and a primary receiver temperature of 4.5K, compared to T-REX, which will have a 86 GHz receiver cooled down to 15K by a HiPTC cryocooler.

[5] T-REX is neither affiliated or sponsored by either BHEX or EHT.

[6] The integration time on the space-ground baseline $\Delta t_{sg} = 10s$ is an order of magnitude smaller due to atmospheric decoherence.

4 Concept of Operations

T-REX will leverage extensive ground supporting infrastructure from the Event Horizon Telescope (EHT) to achieve a VLBI SmallSat platform in Low-Earth Orbit.

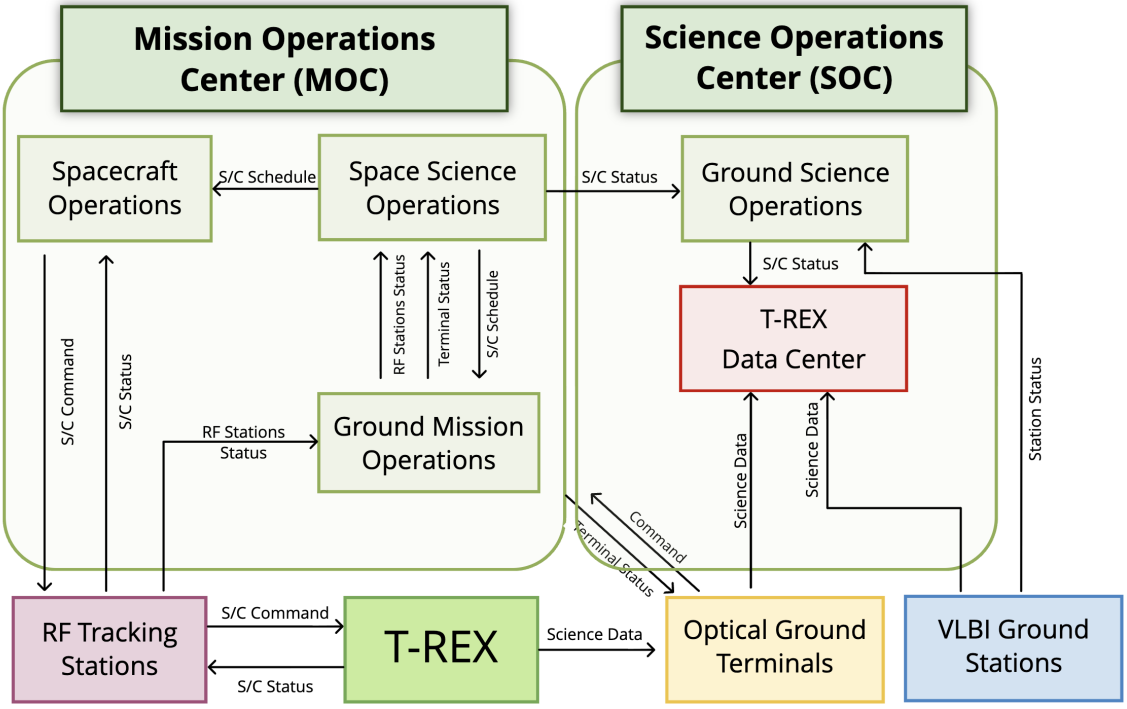

Figure 3: Preliminary Concept of Operations for T-REX and EHT

Ground Science Operations determines the availability of VLBI Ground Stations, Optical Terminals, and RF Tracking Stations and books available communication windows between T-REX and ground infrastructure. Space Science Operations determines the Observing Schedule for T-REX, accounting for atmospheric visibility conditions. Spacecraft Operations creates and relays observing command to RF Tracking Stations, which uplinks the command to T-REX. T-REX slews its antenna, stabilizes, and then observes the target. Consider an integration time $\Delta t = 10s$ on the Space-Ground baseline. T-REX will collect raw electric field voltage data for 22 minutes and then downlink to Optical Ground Terminals, which send their data to the T-REX data center, which correlates interferometric fringes between EHT and T-REX. During correlation, the data is averaged into visibilities over the respective integration time window for each baseline.

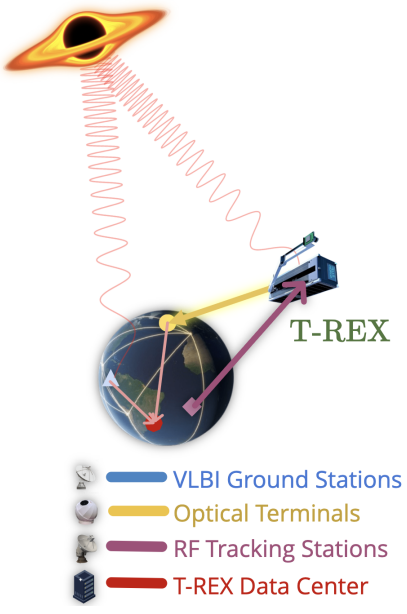

Figure 4: Ground Operations

5 Satellite Architecture

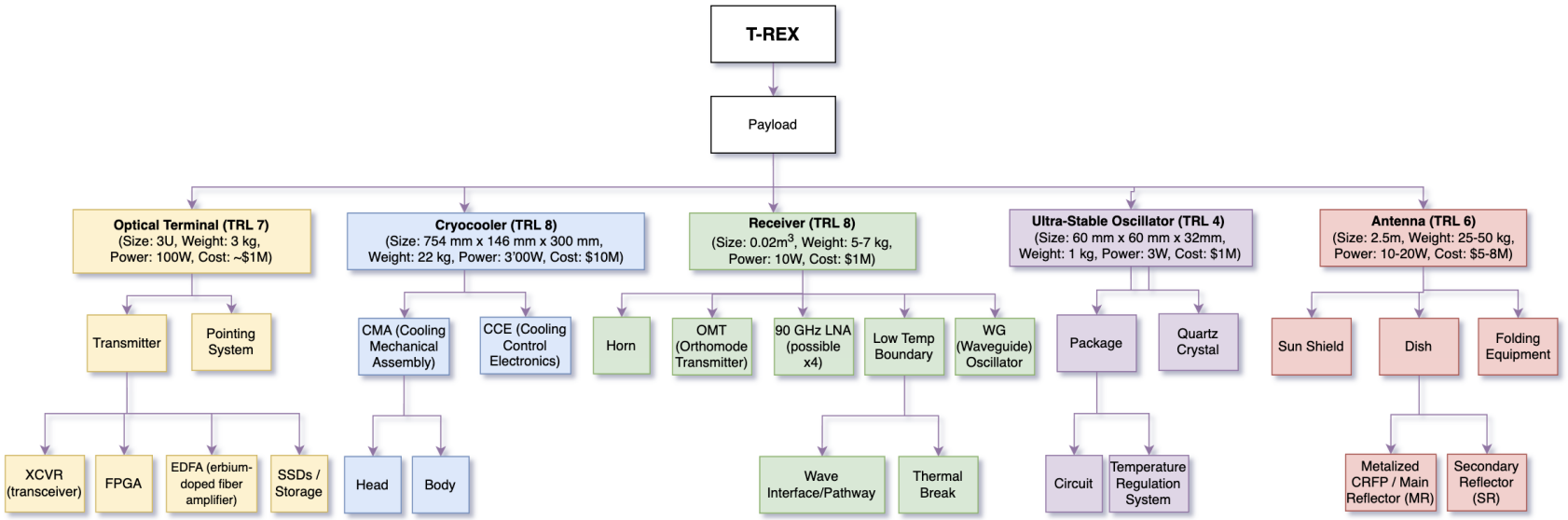

Figure 5: T-REX Instrumentation Breakdown

T-REX's payload consists of several key components: The $d \sim 2.5$m antenna has a primary and secondary reflector which focuses signals onto the primary receiver. T-REX's primary receiver operates at 86 GHz, with each HEMT stage in the receiver expected to dissipate $\sim 5\tilde{}10$ mW [24]. The primary receiver is cryogenically cooled down to sub-20K temperatures by the cryocooler. The T-REX receiver may use HEMT low-noise amplifiers operating at 20K on the 2nd stage of the cryocooler. Assuming two polarizations and 2–3 gain stages per chain, our heat load might be around $\sim 20\tilde{}40$mW at 15K [25]. The Air-Liquide Heat Intercepted Pulse Tube Cooler (HiPTC) has a max input power of 300W, mass 18 kg (both without electronics), and a temperature range of $80 - 100$K for Stage 1 and $10 - 20$K for Stage 2 [26]. The cryocooler has a heat lift $1 - 3$W for Stage 1 and $0.05 - 1W$ for Stage 2 [27]. T-REX requires an exquisite frequency reference system onboard the satellite. Hydrogen masers, which are used in the EHT, are too heavy for a SmallSat. Instead, we determined that the USO under development for LISA will meet the requirements for coherence loss and phase error [21].

6 Instrumentation System Overview

6.1 Antenna

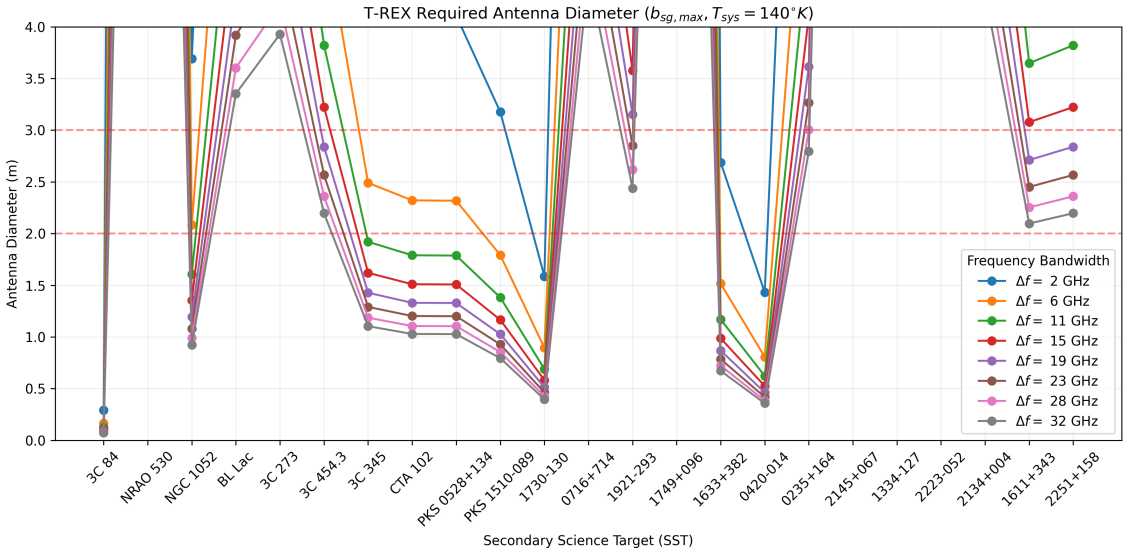

Figure 6: A $2.5m$ diameter antenna resolves most targets at SNR $= 5$ with $T_{sys} = 140K$

To estimate the minimum antenna diameter required to resolve T-REX's radio targets with $SNR > 5$, we estimated all targets as gaussian sources given by[7] [28]

$$V(b) = S \cdot \exp(-\pi^2 b^2 \theta^2 / 4 \ln 2) \tag{6.1}$$

The visibility of the radio targets becomes resolved out at longer baselines, so that bright features are more accessible on shorter baselines. This enables constraints on the thermal noise σ on a given baseline (either Space-Space baseline or Space-Ground baseline), via $\sigma_{SS} < \frac{|V_{SS}|}{SNR}, \sigma_{SG} < \frac{|V_{SG}|}{SNR}$ [29]. This constrains the SEFD via

$$\sigma_{SS} = \frac{1}{\eta_Q}\sqrt{\frac{\text{SEFD}_{\text{BHEX}}\text{SEFD}_{\text{T-REX}}}{2\Delta\nu\Delta t}}, \sigma_{SG} = \frac{1}{\eta_Q}\sqrt{\frac{\text{SEFD}_{\text{T-REX}}\text{SEFD}_{\text{EHT}}}{2\Delta\nu\Delta t}} \tag{6.2}$$

Solving for the required sensitivity of T-REX on a given baseline, we find

$$\text{SEFD}_{\text{T-REX}} = (\sigma_{SS}\eta_Q)^2 \cdot \frac{2\Delta\nu\Delta t}{\text{SEFD}_{\text{EHT}}} \tag{6.3}$$

This enables constraints on the antenna diameter and system temperature T_{sys} via

$$\text{SEFD}_{\text{T-REX}} = \frac{2k_{\text{B}}T^*_{\text{sys}}}{\eta_{\text{A}}A} \rightarrow A = \frac{2kT_{sys}}{\eta_A \text{SEFD}_{\text{T-REX}}} \tag{6.4}$$

[7] A detailed calculation of visibility amplitudes based on individual source morphology will be conducted once T-REX's mission architecture is further constrained.

	D	ϵ	η_A	M	σ	$\Delta\theta$	**Type**
T-REX	2.5m	$\leq 40\mu m$	98%	$25-50$ kg	$5-10\text{kg/m}^2$	$< 30as$	Metal CRFP
BHEX	3.5m	$\leq 40\mu m$	$75-98\%$	25 kg	$5\ \text{kg/m}^2$	$< 30as$	Metal CRFP
HGA	1.8m	$< 85\mu m$	–	12.7 kg	$5\ \text{kg/m}^2$	–	CRFP

Table 1: Comparison of T-REX, BHEX, and Roman HGA Antennas

The system temperature is given by [30]

$$T_{sys} = [T_{rx} + \eta_{eff} T_{source}](1 + r) \tag{6.5}$$

where T_{rx} is the receiver temperature and T_{source} is the brightness temperature of the source, which is given by $T_{source} = \frac{F_{tot} A_{eff}}{2k}$, where F_{tot} is the total flux density of the source and A_{eff} is the effective antenna collecting area.

Observe that the visibility amplitude $V \propto \exp(-b^2)$, where b is the baseline length. Thus, most of T-REX's radio targets are resolved out at baseline lengths exceeding $b > 5G\lambda$. T-REX is able to resolve the extended jet-like or accretion-disk structures on the smaller space-ground baselines b_{sg}. Figure 6 demonstrates that a $d \sim 2.5m$ is sufficient to resolve all secondary science targets with $SNR \geq 5$, regardless of the frequency bandwidth. We find that higher frequency bandwidths decrease the minimum required antenna diameter, with diminishing returns above $\Delta f \sim 9$ GHz. By virtue of having a longer space-space baseline b_{ss}, T-REX also achieves a $\sim 35\mu as$ angular resolution[8].

T-REX may use a metallized CRFP antenna design, similar to BHEX [31]. This design involves an axially symmetric deployable reflector made from a metallized carbon-fiber-reinforced polymer (CFRP) sandwich. The design bonds thin CFRP face sheets to a lightweight honeycomb core, creating a stiff, low-mass panel. A vacuum-deposited aluminum layer provides the RF surface, combining CFRP's mechanical stability with the conductivity of metal. The coating ensures high reflectivity while adding negligible mass. This choice is motivated by extensive spaceflight heritage (e.g., *Planck*, *Herschel*, *Earth-CARE*) and by vendor capability in producing high-precision metallized CFRP reflectors.

For a 2.5 m aperture operating at 86 GHz ($\lambda \approx 3.5$ mm), the metallized CFRP sandwich enables the targeted surface accuracy of $\leq 40\,\mu$m RMS, yielding a Ruze efficiency of $\eta \approx 0.98$, with areal density 5-10 kg m^{-2} and reflector mass between $25-50$ kg: $\eta_A = e^{-4\pi\epsilon/\lambda} \rightarrow \epsilon = \frac{3.5\text{ mm}}{4\pi}\sqrt{-\ln(0.98)} \approx 40\ \mu$m. We are currently conducting a trade study of deployable and rigid parabolic antennas. Although deployable antennas increase potential points of failure and surface RMS error, they mitigate launch fairing size problems, significantly reducing costs. For instance, a 'caketopper' configuration onboard a SpaceX Falcon 9 rocket can easily exceed the cost of the entire mission. A deployable antenna is a unique capability available only at 86 GHz, as it would introduce surface errors that exceed BHEX's $< 40\mu m$ surface error requirements at 345 GHz.

[8]This assumes that T-REX will correlate fringes with BHEX. BHEX (or its partners, including EHT and Smithsonian Astrophysical Observatory) is not affiliated with or endorse T-REX.

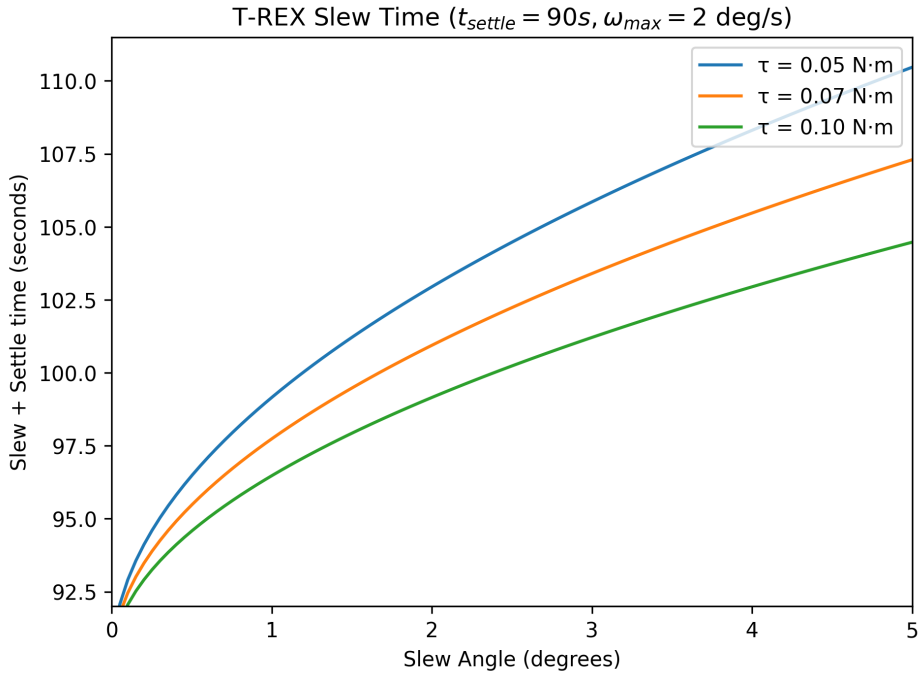

Figure 7: T-REX Slew Times for $\omega_{max} = 2$ deg/s, $t_{settle} = 90s$ for $0° < \theta < 5°$

We now discuss the slew rate of T-REX's Antenna. This will constrain its ability to rapidly respond to astrophysical transients of interest. We use the following simple model. To point at a new radio target and turn by some angle θ, the antenna will: Speed up (accelerate) to a max spin rate ω_{max}, Cruise at that max rate ω_{max}, Slows down (decelerates) to a stop, and finally settle so that pointing is stable (to a pointing accuracy of 30 as).

The four key parameters which characterize the slew rate are as follows: (1) Torque τ: Twist that T-REX's reaction wheels can apply (i.e., how hard the satellite can exert a torque), (2) Inertia I: Rotational Inertia about turn axis, (3) Max Rate ω_{max}: Maximum limit at which satellite is allowed to spin, (4) Settle Time t: A fixed time after deceleration so satellite vibrations relax. We now calculate the slew time in three steps:

1. Time to accelerate to ω_{max}: The angular acceleration of T-REX is $\alpha = \tau/I$. This, in turn, gives the time to accelerate to ω_{max} as $\omega_{max} = \alpha t_{accel} \rightarrow t_{accel} = \omega_{max}/\alpha$.

2. Triangular-Slew Profile: There are two ramps – one accelerating ramp and one decelerating ramp, as the satellite starts and slows its spin. The total angular distance traversed in each ramp is $\theta = \frac{1}{2}\alpha t_{accel}^2$. Thus, for two ramps, we have $\theta_{total} = \alpha t_{accel}^2 = \frac{\omega_{max}^2}{\alpha}$. Thus, $t_{ramp} = \sqrt{\theta/\alpha}$. For a triangular-profile slew, there will be two ramps (one acceleration and one deceleration), so that $t_{slew} = 2 * t_{ramp} = 2\sqrt{\theta/\alpha}$.

3. Trapezoidal-Slew Profile: If the slew angle is sufficiently large ($> 5°$), the telescope will cruise at the max spin rate ω_{max} for a time $t_{cruise} = \frac{\theta_{cruise}}{\omega_{max}}$, where $\theta_{cruise} = \theta - \theta_{accel}$. In that case, the total slew rate will also include the cruise time: $t_{slew} = 2t_{accel} + t_{cruise}$.

6.2 Primary Receiver

The purpose of T-REX's primary receiver is to accept radio signals from black hole targets and ultimately convert them into an analog signal which can be fed into the digital backend. In particular, the primary receiver consists of the following components: a corrugated horn, an orthomode transducer (OMT), noise calibration injection, low-noise amplifiers, and mixers coupled to the local oscillator. T-REX's antenna consists of a primary and secondary reflector. The secondary reflector focuses radio signals into the horn, which channels them into a waveguide which meets the OMT. The OMT splits the incoming 86 GHz radio signal into two linear polarizations (Pol-1 and Pol-2), enabling polarimetric science on black hole targets. The noise calibration signal is an injection which enables T-REX to calibrate how many watts are being received from the radio target. The low-noise amplifiers (LNA) are cryogenically cooled to 15K by a High Pulse Tube Cryocooler (Hi-PTC) with spaceflight heritage. The High-Electron Mobility Transfer (HEMT) LNAs amplify the incoming 86 GHz signal with a potential $\sim 40-60$ dB cold gain. The mixers convert the 86 GHz signal into $4-12$ GHz intermediate frequency signals which can be routed to the digital backend for signal processing and conversion from an analog signal to a digital signal. The mixers are coupled to the frequency reference system for T-REX, which we have tentatively determined to be the ultra-stable oscillator (USO) being developed for NASA/ESA's LISA mission, with Van Allen Deviation $\sigma_y = 8e-15$ for $t = 10s$.

6.3 Cryocooler

T-REX has tentatively selected Air Liquide's Heat-Intercepted Pulse-Tube Cooler.

	P	M	T	Q
Hi-PTC (Stage 1)	300W	18kg	$80-100K$	$1-3W$
Hi-PTC (Stage 2)	–	–	$10-20$K	$0.05-1W$

Table 2: Input Power, Mass, Temperature Range, and Heat Lift for T-REX's Cryocooler

6.4 Digital Backend

The input and output of the primary receiver is a 86 GHz signal and a 4-12 GHz IF signal, respectively. This IF signal stream is fed into the digital backend (DB), which converts the analog signals into digital signals which can be downlinked to ground. The digital backend essentially performs the following signal processing algorithm: it samples the raw analog signal from the receiver at some discrete frequency $f_s \geq 2f$ obeying the Nyquist-Shannon Sampling Theorem. If the DB employs 1-bit quantization, it records only the sign of the signal voltage, whereas 2-bit quantization also records the strength of the signal as a low or high positive/negative signal. The quantization efficiency η_A(amount of analog signal retained after digitization) is given by $\eta_Q(N_{bit}) \sim 1 - \frac{\pi}{2}2^{-2N_{bit}} \rightarrow n_Q(1 \text{ bit}) \sim 63\%, n_Q(2 \text{ bit}) \sim 88\%$[9]. We are conducting trade studies to determine the quantization scheme for T-REX, accounting for ground coverage, onboard storage, and downlink rate.

[9]The relative cross-correlation η_A is given by $\eta = \sqrt{\eta_1 \eta_2}$

6.5 Ultra-Stable Oscillator

Very Long Baseline Interferometry (VLBI) involves the combination of multiple radio telescopes into a larger 'virtual' telescope with a smaller effective angular resolution given by $\theta \sim \lambda/D$. VLBI operates by combining radio signals from widely-separated telescopes. A highly accurate frequency reference system is required to coherently add radio signals from different telescopes and achieve higher SNR. EHT uses highly precise atomic clocks such

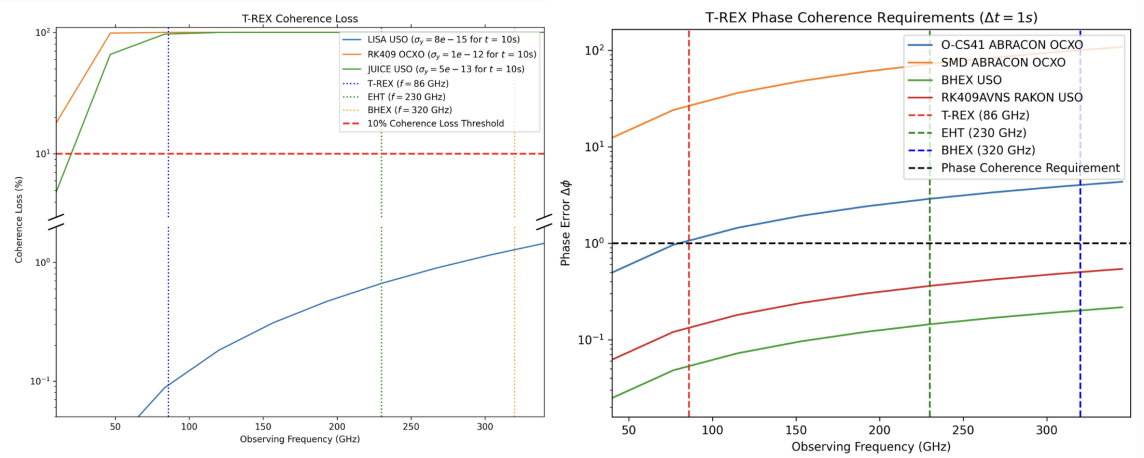

Figure 8: T-REX Coherence Loss and Phase Coherence Requirements

as hydrogen masers, which can achieve frequency stabilities on the order of ~ 1 in every 10^{-14} over $\Delta t = 10s$ of integration time. We now present constraints on T-REX's Allan Deviation if it seeks to achieve a Coherence Loss $L \leq 10\%$ and phase error $\Delta\phi < 1$ radian. These constraints are required to resolve black hole targets at $SNR > 5$ and achieve phase coherence when correlating fringes between T-REX, BHEX and EHT.

In Figure 9, we plot the Coherence Loss as a function of Observing Frequency for three frequency reference systems: Ultra-Stable Oscillators (USO) for ESA's Jupiter Icy Moons Explorer (JUICE) mission and NASA's Laser Interferometer Space Antenna (LISA), as well as the Rakon RK409 Oven Controlled Crystal Oscillator (OCXO). RK409 OCXO has an Allan Deviation $\sigma_y = 10^{-12}$ for $\Delta t = 10s$; JUICE USO has $\sigma_y = 5 \cdot 10^{-13}$ for $\Delta t = 10s$. The USO being developed for LISA is projected to have $\sigma_y = 8 \cdot 10^{-15}$. From this limited trade space of frequency reference systems, it seems that the LISA USO achieves the $L < 10\%$ coherence loss constraint required for T-REX to resolve black hole targets at $SNR > 5$.

Figure 9 also plots the Phase Error $\Delta\phi$ for four frequency reference systems: O-CS41 OCXO, SMD OCXO, BHEX USO, and the RK409 USO. We compute the phase error by

$$\Delta\phi = 2\pi \cdot f_{obs} \cdot \sigma_t, \sigma_t = \sigma_y \cdot \Delta t \tag{6.6}$$

where f_{obs} is the observing frequency, σ_t is the timing jitter, which is proportional to the Allan Deviation σ_y and the integration time Δt. A phase error of $\Delta\phi < 1$ rad is required to achieve phase coherence and achieve $SNR > 5$. We find that for an integration time of $\Delta t = 1s$, O-CS41 OCXO seems to barely meet this constraint, whereas the BHEX USO and RK409 USO exceed the phase error requirement.

6.6 Optical Terminal

T-REX faces limited ground coverage from its LEO orbit, a problem exacerbated Data Downlinking is a significant problem due to the sheer amount of data generated by VLBI. Assuming a $f_{duty} = 0.5$ duty cycle for a 5400 s (90-minute) orbit in LEO, T-REX would be observing a black hole target for

$$T_{\text{observe}} \;=\; \tfrac{1}{2}\,T_{\text{orbit}} \;=\; 2700\,\text{s},$$

Assuming two orthogonal polarizations ($N_{\text{pol}} = 2$) with Nyquist factor ($N_{\text{Nyquist}} = 2$) over $\Delta\nu = 16$ GHz, the raw data-gathering rate is

$$r \;=\; N_{\text{bit}} \times 16 \times 10^9 \times N_{\text{pol}} \times N_{\text{Nyquist}} \;=\; N_{\text{bit}} \times 16 \times 10^9 \times 2 \times 2.$$

Thus for $N_{\text{bit}} = 1$, $r = 32$ Gb/s, and for $N_{\text{bit}} = 2$, $r = 64$ Gb/s. Given $T_{observe} = 2700s$ and converting to gigabytes (GB), we obtain the plots shown below.

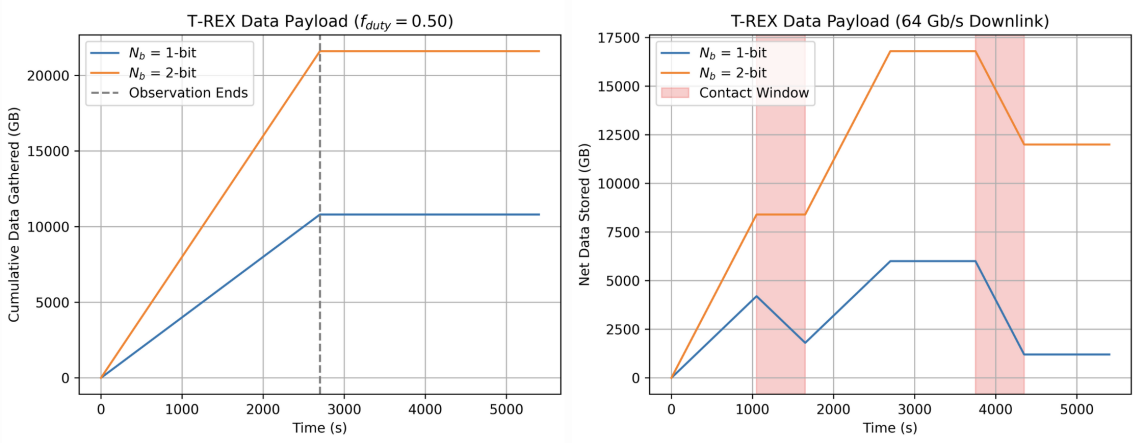

Figure 9: Data Payload for T-REX with (Right) and without (Left) Optical Downlink

Figure 10 demonstrates cumulative data stored onboard T-REX given a 64 Gb/s downlink rate (i.e., using a TBIRD Downlink System). In the plateau chart, data accumulates linearly up to T_{observe} and then remains flat for the rest of the orbit.

In the net-data chart we introduce two 600s ground-contact windows (centered at 25 and 75 of the orbit) during which 64 Gb/s are downlinked (i.e., lost from onboard storage). We compute the cumulative "lost" bits by integrating $R_{\text{loss}} = 64 \times 10^9$ b/s across each contact window, convert to GB, and subtract from the onboard total. The resulting curves thus show how much data remains stored onboard over time for both N_{bit} settings, with the shaded regions marking the ground-station contact periods. Fig 3 demonstrates the impact of a $D_r = 20$ Gb/s downlink rate on the Net Data Stored onboard the satellite.

Due to the lack of ground coverage from low-earth orbit, T-REX will require at least five receiving stations on earth. Below is a sample of potential data downlink stations. We are currently in the process of identifying potential groundlink stations. The University of Western Ontario's receiving station may also be a potential ground station.

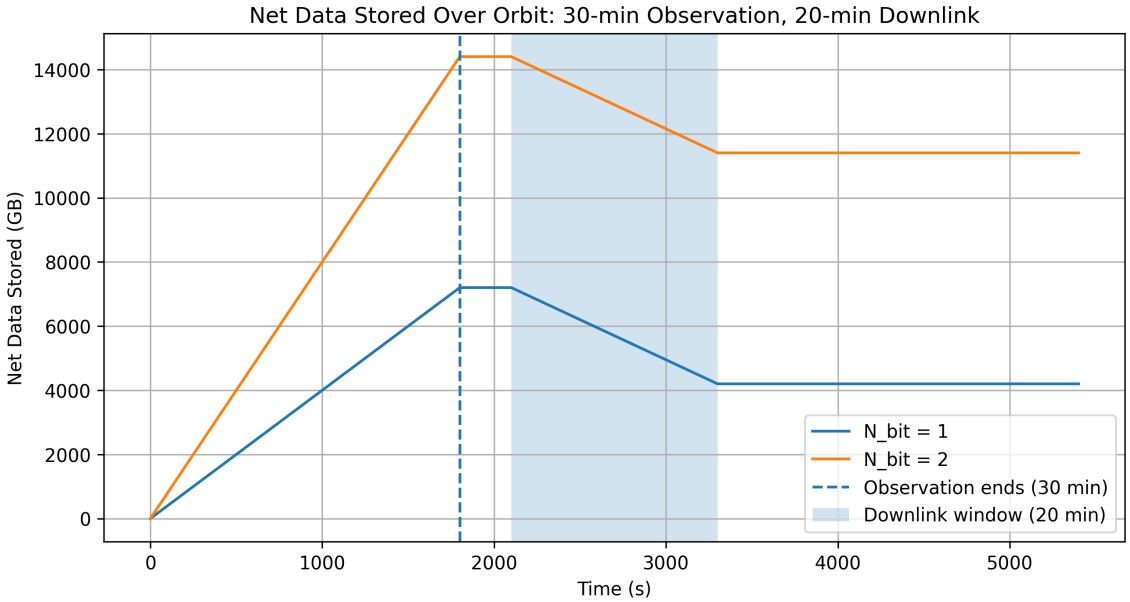

Figure 10: T-REX Data Payload for $\Delta\nu = 8$ GHz, $T_{obs} = 30$ min, $D_r = 20$ Gb/s

After potential ground stations are finalized, we will determine our total ground contact time as a function of our orbital configuration in LEO. A preliminary example of such a plot looks as follows. The total ground coverage, in addition to the duty cycle and total data payload generated over one orbit will constrain the minimum data downlink rate. The team is currently optimizing the number and placement of optical downlink receiving stations on Earth. For the the time being, limited ground coverage can be addressed with the dual approach of physical onboard storage via SSDs and optimization of true anomaly to maximize ground coverage.

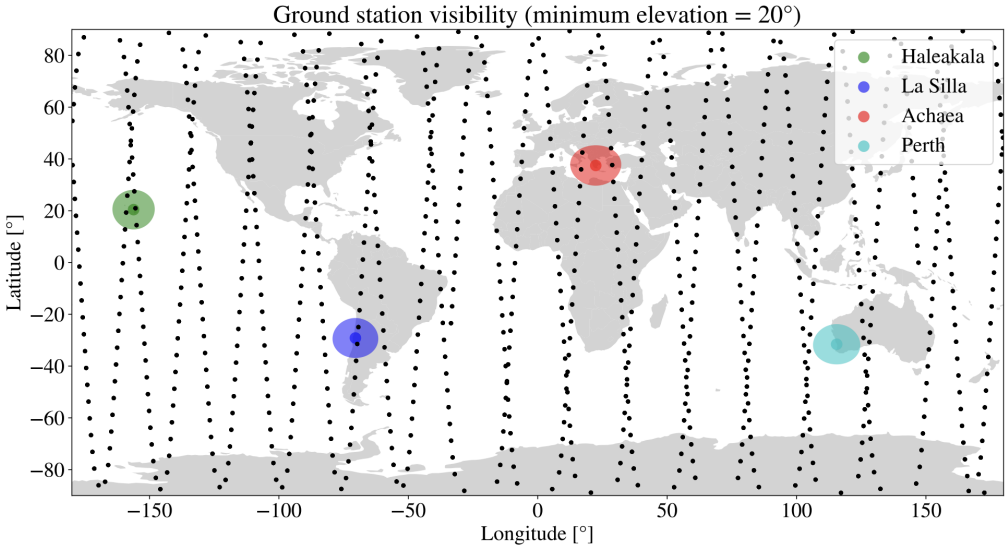

Figure 11: Preliminary Ground Coverage for T-REX for 4 Sample Receiving Stations

7 Temporal Resolution Requirements

T-REX's primary science objective is to capture the first video of Sgr A^*. To do so, T-REX must achieve $> 50\%$ (u, v) coverage on sub-ISCO timescales (< 30 minutes) [32]. As T-REX rapidly orbits in LEO, it faces the following constraint on the integration time to prevent a phase wrap on the visibility measurement:

$$\tau < \frac{1}{\omega D_\lambda \theta_{\text{FOV}}} \tag{7.1}$$

The angular velocity for a satellite in Low-Earth Orbit is $\omega = \frac{2\pi}{P} = \frac{2\pi}{1.5 \text{ hr} \cdot \frac{3600s}{1\text{hr}}} = 1.16 \times 10^{-3} rad/s$. T-REX's Space-Ground baseline length varies between

$$0.11G\lambda < b_{sg} < 3.5G\lambda, \theta_{FOV} = 180\mu as \tag{7.2}$$

Given that the event horizon of Sgr A^* is on the order of 50 μas, we assume a conservative $\theta_{FOV} = 180\mu as$ which would be sufficient to observe accretion disk phenomenon surrounding the black hole, but probably insufficient for observing jets produced by the black hole. Convert θ_{FOV} to radians:

$$180\mu as = 180 \cdot 10^{-6} as \cdot 4.8 * 10^{-6} \frac{rad}{as} = 8.64 \cdot 10^{-10} rad \tag{7.3}$$

Thus, the maximum integration time for T-REX is ~ 275 seconds:

$$\tau_{max} < \frac{1}{(1.2 \cdot 10^{-3} rad/s)(3.5G\lambda)(8.64 \cdot 10^{-10} rad)} \sim 4.5 \text{ minutes} \tag{7.4}$$

To calculate the minimum integration time, we use the geometric mean of the individual telescope sensitivities.

$$\tau_{\text{min}} = \frac{\text{SEFD}_1 \text{SEFD}_2}{2\Delta\nu} \left(\frac{1}{\eta_{\text{Q}} \sigma_{\text{nom}}} \right)^2 \tag{7.5}$$

By using the representative values $T_{rx} = 15K, \eta_{ff} = 0.95, \eta_A = 0.85, r = 1, F_{tot} \sim 2 \pm 0.2Jy \rightarrow \text{SEFD}_{\text{T-REX}} = \frac{2kT^*_{sys}}{\eta_A A} \sim 32,000$ Jy, we find $\text{SEFD}_{\text{T-REX}} = \frac{2kT^*_{sys}}{\eta_A A} \sim 32,000$ Jy. Since $\text{SEFD}_{\text{EHT}} = 6000$ Jy, $\Delta\nu = 16$ GHz, $\sigma_{nom} = 10$ mJy, and $\eta_Q = 0.75$, we obtain $\tau_{min} = 106.4s$. Thus, T-REX has the following maximum and minimum integration times for its Space-Ground baseline:

$$106.4s < \tau_{GS} < 275s \tag{7.6}$$

The (u, v) plane has complex conjugate symmetry, meaning that when one point is sampled, the antipodal point is also sampled. Therefore, in half an orbital period almost all the (u, v) plane is sampled, and in a quarter of a period, T-REX will fill half of the spatial scales it will sample on the fourier domain. Following Tamar et. al. (2025) [19], we thus define temporal resolution of T-REX via:

$$t_{res} = \frac{P}{4} \rightarrow \frac{90}{4} = 22.5 \text{ minutes} \tag{7.7}$$

T-REX's temporal resolution satisfies the < 30 minute constraint for time-resolving Sgr A*. By leveraging its LEO VLBI platform, T-REX will be nominally capable of capturing the first video of Sgr A*. Only T-REX, by virtue of its LEO orbit – as opposed to EHT or BHEX – can satisfy this temporal resolution constraint.

8 Parameter Estimation from Black Hole Movies

By capturing a video of Sgr A*, T-REX will enable parameter estimation on Sgr A*'s mass, spin, luminosity, accretion rate, polarization, and magnetic field [32].

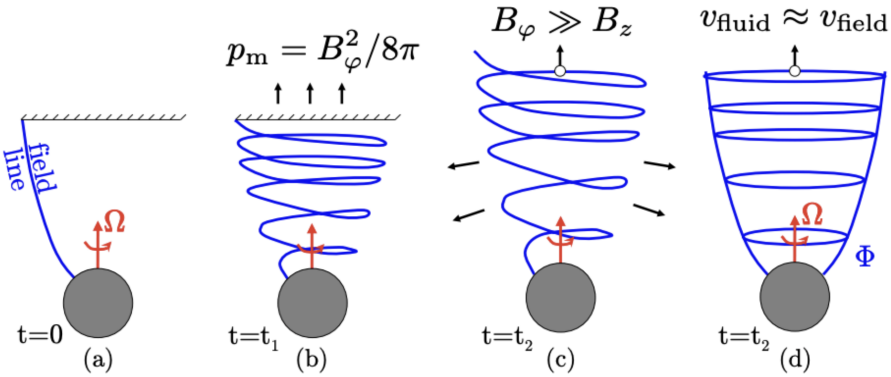

Figure 12: Azimuthal B_ϕ and Vertical B_z Magnetic Fields around Black Hole [33]

Accretion disks form when gas with angular momentum spirals toward a compact object but cannot fall directly in. Instead, the gas settles into orbits, moving with Keplerian velocity $\Omega(R) = \sqrt{\frac{GM}{R^3}}$. Thus, material closer to the black hole moves faster than material farther out. In a video of the accretion flow, this differential motion can be detected as brightness patterns or hot spots that orbit with time, enabling direct constraints on the black hole mass M. One can place a constraint on the black hole's spin from this, as follows. For a Kerr black hole with spin parameter $a = \chi M$ and observer inclination i, the Bardeen coordinates for the shadow boundary on the image plane is [34]

$$\alpha = -\frac{\xi}{\sin i}, \quad \beta = \pm\sqrt{\eta + a^2\cos^2 i - \xi^2\cot^2 i} \tag{8.1}$$

with critical photon constants (from spherical photon orbits at radius r) [35]

$$\xi(r) = \frac{r^2(r-3M) + a^2(r+M)}{a(M-r)}, \quad \eta(r) = \frac{r^3\left(4a^2M - r(r-3M)^2\right)}{a^2(M-r)^2} \tag{8.2}$$

Fitting these points with a best-fit circle gives a dimensionless scale $\mathcal{F}(a,i)$. Then

$$M = \frac{c^2 D}{G}\frac{\theta_{\rm sh}}{\mathcal{F}(a,i)} \tag{8.3}$$

For $a = 0$, a Schwarzschild black hole has $\mathcal{F} = 2\sqrt{27}$. In practice one solves jointly for M and a since $\mathcal{F}$ depends weakly on (a,i) while the displacement/asymmetry below depends strongly. In addition to orbiting the black hole, the gas will lose angular momentum and drift inward, quantified by the mass accretion rate [36]:

$$\dot{M} = -2\pi R\rho u_R \tag{8.4}$$

ρ is the surface density and u_R is the radial velocity. The disk will become brighter when more matter flows into the black hole. Therefore, the video will show changes in luminosity directly reflecting fluctuations in the accretion rate. The luminosity is given by: $L = \eta \dot{M} c^2$. η is the efficiency of energy conversion. Thus, when a video shows the disk brightening or dimming, we are directly observing changes in the accretion rate and energy release. The light seen through the video shows the gravitational energy of infalling gas converted into radiation. The evolution of the disk is controlled by viscosity, which transports angular momentum outward and allows accretion to happen. The torque between rings is given by

$$T(R) = 2\pi\nu\rho R^3 \frac{d\Omega}{dR} \tag{8.5}$$

This sets the rate at which the disk spreads. In a time-lapse video, we can see this spreading as outer regions slowly brighten while inner regions dim, showing angular momentum carried outward. Luminosity changes on short timescales (such as flares, flickers, or periodic brightening) will reveal instabilities in the flow and can be used to estimate the viscosity parameter ν. Longer variations will correspond to the global redistribution of mass and momentum predicted by these equations. Therefore, by watching how the disk's brightness and structure evolve over time through a video, the TREX satellite provides a direct observational test of the fundamental physics of accretion: the conversion of orbital energy into light, the inward transport of mass, and the outward transport of angular momentum. Continuous video monitoring links the changing luminosity of the disk directly to changes in accretion physics.

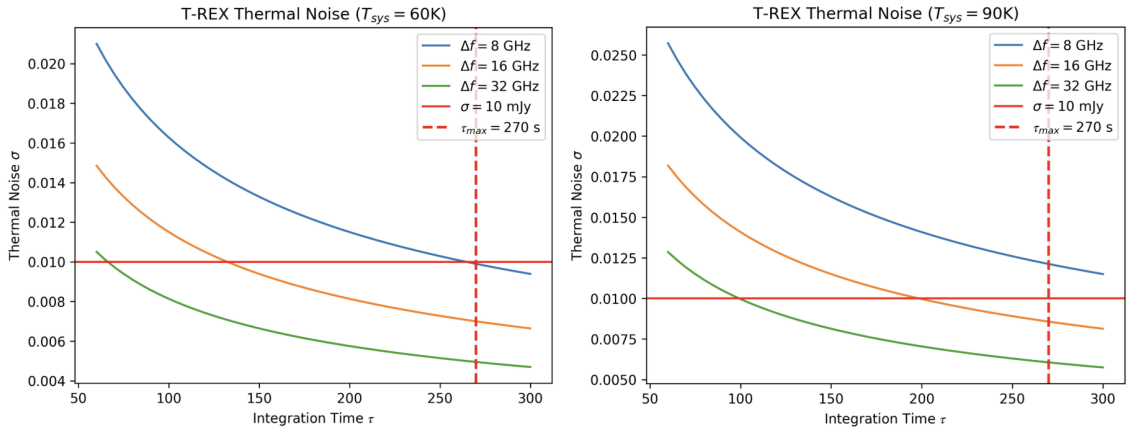

Figure 13: Thermal Noise Plots at $T_{sys} = 60K$ and $T_{sys} = 60K$ for T-REX

Acknowledgements

Thank you to Prof. Brendan Keith, the Institutional PI of T-REX, for supporting the proposal. In addition, we thank our collaborators for their insight and guidance on the mission concept: Lucas Anderson, Jeremy Goodman, Krista Lynne Smith, Travis Fischer, Joe Lazio, and Kimberly Weaver. We also thank the students Ariel Baksh and Tsogt Enkhbat for their contributions to the proposal.

References

[1] E. H. T. Collaboration *et al.*, "First m87 event horizon telescope results. i. the shadow of the supermassive black hole," *arXiv preprint arXiv:1906.11238*, 2019.

[2] N. A. of Sciences Engineering and Medicine, "Pathways to discovery in astronomy and astrophysics for the 2020s," tech. rep., National Academies of Sciences, Engineering, and Medicine, Washington, DC, 2021.

[3] A. Shlentsova, F. Roelofs, S. Issaoun, J. Davelaar, and H. Falcke, "Imaging the event horizon of m87* from space on different timescales," *Astronomy & Astrophysics*, vol. 686, p. A154, 2024.

[4] K. Satapathy, D. Psaltis, F. Özel, L. Medeiros, S. T. Dougall, C.-K. Chan, M. Wielgus, B. S. Prather, G. N. Wong, C. F. Gammie, *et al.*, "The variability of the black hole image in m87 at the dynamical timescale," *The Astrophysical Journal*, vol. 925, no. 1, p. 13, 2022.

[5] A. King, J. Pringle, R. G. West, and M. Livio, "Variability in black hole accretion discs," *Monthly Notices of the Royal Astronomical Society*, vol. 348, no. 1, pp. 111–122, 2004.

[6] M. Afrin and S. G. Ghosh, "Eht observables as a tool to estimate parameters of supermassive black holes," *Monthly Notices of the Royal Astronomical Society*, vol. 524, no. 3, pp. 3683–3691, 2023.

[7] V. Perlick and O. Y. Tsupko, "Calculating black hole shadows: review of analytical studies," *Physics Reports*, vol. 947, pp. 1–39, 2022.

[8] L. Dey, A. Gopakumar, M. Valtonen, S. Zola, A. Susobhanan, R. Hudec, P. Pihajoki, T. Pursimo, A. Berdyugin, V. Piirola, *et al.*, "The unique blazar oj 287 and its massive binary black hole central engine," *Universe*, vol. 5, no. 5, p. 108, 2019.

[9] J.-W. Chen and Y. Zhang, "Gravitational wave detection from oj 287 via a pulsar timing array," *Monthly Notices of the Royal Astronomical Society*, vol. 481, no. 2, pp. 2249–2260, 2018.

[10] M. J. Valtonen, L. Dey, A. Gopakumar, S. Zola, S. Komossa, T. Pursimo, J. L. Gomez, R. Hudec, H. Jermak, and A. V. Berdyugin, "Promise of persistent multi-messenger astronomy with the blazar oj 287," *Galaxies*, vol. 10, no. 1, p. 1, 2021.

[11] B. Keith, A. Khadse, and S. E. Field, "Learning orbital dynamics of binary black hole systems from gravitational wave measurements," *Physical Review Research*, vol. 3, no. 4, p. 043101, 2021.

[12] R. D. Blandford and R. L. Znajek, "Electromagnetic extraction of energy from kerr black holes," *Monthly Notices of the Royal Astronomical Society*, vol. 179, pp. 433–456, 1977.

[13] A. G. Pacholczyk, *Radio Astrophysics: Nonthermal Processes in Galactic and Extragalactic Sources*. San Francisco: Freeman, 1970.

[14] F. Yuan and R. Narayan, "Hot accretion flows around black holes," *Annual Review of Astronomy and Astrophysics*, vol. 52, pp. 529–588, 2014.

[15] J. D. Hogg and C. S. Reynolds, "The influence of accretion disk thickness on the large-scale magnetic dynamo," *The Astrophysical Journal*, vol. 861, no. 1, p. 24, 2018.

[16] L. I. Gurvits, "Space vlbi: from first ideas to operational missions," *Advances in Space Research*, vol. 65, no. 2, pp. 868–876, 2020.

[17] E. R. Benton and E. Benton, "Space radiation dosimetry in low-earth orbit and beyond," *Nuclear Instruments and Methods in Physics Research Section B: Beam Interactions with Materials and Atoms*, vol. 184, no. 1-2, pp. 255–294, 2001.

[18] E. Peretz, P. Kurczynski, M. D. Johnson, J. Houston, T. K. Sridharan, J. Wang, P. Galison, R. Gamble, D. Marrone, S. Noble, *et al.*, "The black hole explorer: Astrophysics mission concept engineering study report," in *Space Telescopes and Instrumentation 2024: Optical, Infrared, and Millimeter Wave*, vol. 13092, pp. 886–917, SPIE, 2024.

[19] A. Tamar, B. Hudson, and D. Palumbo, "Orbit design for mitigating interstellar scattering effects in earth-space vlbi observations of sgr a," *arXiv preprint arXiv:2504.07892*, 2025.

[20] M. D. Johnson, K. L. Bouman, L. Blackburn, A. A. Chael, J. Rosen, H. Shiokawa, F. Roelofs, K. Akiyama, V. L. Fish, and S. S. Doeleman, "Dynamical imaging with interferometry," *The Astrophysical Journal*, vol. 850, no. 2, p. 172, 2017.

[21] G. Heinzel, K. Danzmann, A. Marin, F. Guzman, A. Sutton, D. Schuetze, G. Dixon, and et al., "The lisa frequency reference: ultra-stable oscillator development and performance," *Classical and Quantum Gravity*, vol. 37, no. 21, p. 215018, 2020.

[22] B. v. d. Kolk, J. Pijnenburg, M. de Graauw, J. van Harten, and M. van Vliet, "Ultra-stable oscillator for the juice mission: flight model performance and lessons learned," in *International Conference on Space Optics — ICSO 2022*, vol. 12180, p. 121803F, SPIE, 2022.

[23] A. R. Thompson, J. M. Moran, and G. W. Swenson, *Interferometry and Synthesis in Radio Astronomy*. Cham, Switzerland: Springer, 3rd ed., 2017.

[24] M. W. Pospieszalski, "Cryogenic low-noise amplifiers," *IEEE Microwave Magazine*, vol. 18, no. 6, pp. 42–54, 2017.

[25] C. E. Tong, K. Akiyama, P. Grimes, M. Honma, J. Houston, M. D. Johnson, D. P. Marrone, H. Rana, and Y. Uzawa, "Receivers for the black hole explorer (bhex) mission," in *Space Telescopes and Instrumentation 2024: Optical, Infrared, and Millimeter Wave*, vol. 13092, pp. 2212–2218, SPIE, 2024.

[26] F. Berger, I. Charles, J. Rey, M. Thales, A. Della Corte, and P. Duret, "Air liquide high-capacity heat intercepted pulse tube cooler for space applications," in *International Conference on Space Optics — ICSO 2016*, vol. 10562, p. 105622L, SPIE, 2017.

[27] Air Liquide Advanced Technologies, "Active cryo cooling for space application: Pulse tube coolers (brochure)." https://advancedtech.airliquide.com/sites/alat/files/2022-10/pulsetube_brochure_en_08.21_sd.pdf, Aug. 2021. Brochure.

[28] J. P. Berger and D. Segransan, "An introduction to visibility modeling," *New Astronomy Reviews*, vol. 51, no. 8-9, pp. 576–582, 2007.

[29] M. D. Johnson, K. Akiyama, R. Baturin, B. Bilyeu, L. Blackburn, D. Boroson, A. Cárdenas-Avendaño, A. Chael, C.-k. Chan, D. Chang, *et al.*, "The black hole explorer: Motivation and vision," in *Space Telescopes and Instrumentation 2024: Optical, Infrared, and Millimeter Wave*, vol. 13092, pp. 821–872, SPIE, 2024.

[30] D. W. Pesce, L. Blackburn, R. Chaves, S. S. Doeleman, M. Freeman, S. Issaoun, M. D. Johnson, G. Lindahl, I. Natarajan, S. N. Paine, *et al.*, "Atmospheric limitations for high-frequency ground-based very long baseline interferometry," *The Astrophysical Journal*, vol. 968, no. 2, p. 69, 2024.

[31] T. Sridharan, R. Lehmensiek, D. Marrone, P. Cheimets, M. Freeman, P. Galison, J. Houston, M. Johnson, and M. Silver, "The black hole explorer (bhex): Preliminary antenna design," in *Space Telescopes and Instrumentation 2024: Optical, Infrared, and Millimeter Wave*, vol. 13092, pp. 2205–2211, SPIE, 2024.

[32] D. C. Palumbo, S. S. Doeleman, M. D. Johnson, K. L. Bouman, and A. A. Chael, "Metrics and motivations for earth–space vlbi: Time-resolving sgr a* with the event horizon telescope," *The Astrophysical Journal*, vol. 881, no. 1, p. 62, 2019.

[33] S. W. Davis and A. Tchekhovskoy, "Magnetohydrodynamics simulations of active galactic nucleus disks and jets," *Annual Review of Astronomy and Astrophysics*, vol. 58, no. 1, pp. 407–439, 2020.

[34] S. C. Garmier, "The shadow of a rotating black hole," *ETH Zurich Thesis*, 2021.

[35] A. Chael, M. D. Johnson, and A. Lupsasca, "Observing the inner shadow of a black hole: a direct view of the event horizon," *The Astrophysical Journal*, vol. 918, no. 1, p. 6, 2021.

[36] R. Narayan and E. Quataert, "Black hole accretion," *Science*, vol. 307, no. 5706, pp. 77–80, 2005.